

Synthesis of Magnetic Sonophotocatalyst and its Enhanced Biodegradability of Organophosphate Pesticide

Meng Lirong, Shi Jianjun,* Zhao Ming, and He Jie

School of Chemical Engineering, Anhui University of Science and Technology, Huainan, Anhui 232001, P.R. China

*E-mail: jjshi@aust.edu.cn

Received July 26, 2014, Accepted August 14, 2014

A magnetic sonophotocatalyst $\text{Fe}_3\text{O}_4@\text{SiO}_2@\text{TiO}_2$ is synthesized for the enhanced biodegradability of organophosphate pesticide. The as-prepared catalysts were characterized using different techniques, such as X-ray diffraction (XRD) and transmission electron microscopy (TEM). The radial sonophotocatalytic activity of $\text{Fe}_3\text{O}_4@\text{SiO}_2@\text{TiO}_2$ nanocomposite was investigated, in which commercial dichlorvos (DDVP) was chosen as an object. The degradation efficiency was evaluated in terms of chemical oxygen demand (COD) and enhancement of biodegradability. The effect of different factors, such as reaction time, pH, the added amount of catalyst on COD_{Cr} removal efficiency were investigated. The average COD_{Cr} removal efficiency reached 63.13% after 240 min in 12 L sonophotocatalytic reactor (catalyst 0.2 g L^{-1} , pH 7.3). The synergistic effect occurs in the combined sonolysis and photocatalysis which is proved by the significant improvement in COD_{Cr} removal efficiency compared with that of solo photocatalysis. Under this experimental condition, the $\text{BOD}_5/\text{COD}_{\text{Cr}}$ ratio rose from 0.131 to 0.411, showing a remarkable improvement in biodegradability. These results showed that sonophotocatalysis may be applied as pre-treatment of pesticide wastewater, and then for biological treatment. The synthesized magnetic nanocomposite had good photocatalytic performance and stability, as when it was used for the fifth time, the COD_{Cr} removal efficiency was still about 62.38%.

Key Words : Sonophotocatalysis, Magnetic nanocomposite, Titanium dioxide, Biodegradability, Organophosphate pesticide

Introduction

Organophosphate pesticides have been widely used for agricultural purposes due to their relatively low price and effective ability to control pests, weeds and diseases.¹ Dimethyl dichlorovinyl phosphate (DDVP) is an efficient broad-spectrum organophosphate pesticide. However, the extensive and indiscriminate use of such pesticides in agricultural production, postharvest, and storage may result in ubiquitous pollution in the diet and ground water, which are medium poisonous if inhaled, swallowed or absorbed through skin.^{2,3} These contaminants are usually non-biodegradable, toxic and quite persistent in the environment.⁴ As a result, there is an urgent need to develop an effective treatment method for the removal of DDVP from the polluted water. Over the past 20 years, different treatment technologies such as biodegradation, ultrasonication, adsorption, and heterogeneous photocatalysis have been studied on the removal of pesticide contamination.⁴⁻⁷ Among the above various treatment technologies, TiO_2 photocatalysis has been proven as a promising technology for pesticide contamination treatment.⁸⁻¹⁰ However, the separation and recovery of photocatalyst are difficult, which limit the application of TiO_2 slurry reactor in practical application.¹¹

Many researches have been carried out by immobilizing TiO_2 onto magnetic substrates, which provide a very convenient approach for the separation and recycling of the photocatalyst.^{12,13} Linley *et al.* used tetrabutyl titanate as

titanium sources, obtained magnetic rattle-type nanostructure $\text{Fe}_3\text{O}_4/\text{TiO}_2$ photocatalyst with high specific surface area and more catalytic reaction sites than pure TiO_2 .¹⁴ However, Fe_3O_4 nanoparticles (NPs) are susceptible to air oxidation. Moreover, directly introducing Fe_3O_4 as the core of the $\text{Fe}_3\text{O}_4@\text{TiO}_2$ nanostructure would produce photodissolution problems. Many researches indicated that the photodissolution problem could be prevented by introducing a passivation layer between the Fe_3O_4 core and the TiO_2 shell.¹⁵⁻¹⁷ Yang *et al.* obtained the core-shell structured $\text{Fe}_3\text{O}_4@\text{C}@\text{TiO}_2$ magnetic nanocomposite with enhanced photocatalytic activity by combining hydrothermal method with calcination.¹⁶ Fan *et al.* designed a well-defined core-shell-shell structured $\text{Fe}_3\text{O}_4/\text{SiO}_2/\text{TiO}_2$ nanocomposite by a facile hydrothermal synthetic method.¹⁷ Therefore, the designed magnetic core-shell photocatalyst possesses a uniform size, good structural stability, high surface area, excellent magnetic separation, and remarkable photocatalytic performance.

Recently, sonophotocatalysis has been receiving attention as a promising technique for the treatment of hazardous organic contaminants in water. Many studies have been reported on combining ultrasound with UV light irradiation in the presence of TiO_2 and sonophotocatalysis can enhance the efficiency of semiconductor mediated degradation of organic contaminants synergistically.¹⁸⁻²⁰ To the best of our knowledge, the combination of radial ultrasound and magnetic core-shell photocatalyst was seldom reported. Radial ultrasound can increase the distribution area of ultrasound

wave, thus increasing the amounts of the reactive radical species. Moreover, radial ultrasound may disperse the aggregated catalyst particles, thereby increasing active surface area. Furthermore, radial ultrasound is also beneficial to the activation of the reused photocatalysis. Contrast to conventional ultrasound technique, radial ultrasound technique could be more suitable for high concentration and large-scale wastewater treatment. By inducing magnetic core-shell photocatalyst into the radial sonophotocatalytic degradation of organophosphate pesticide, the benefits of core-shell photocatalysts are retained, while also endowing the particles with magnetic separability and recycled use without loss in activity.¹⁴ However, the high operating costs of sonophotocatalysis are still a significant drawback for industrial applications. For instance, complete mineralization of organophosphate pesticide effluents usually requires longer periods of treatment and a large number of catalysts.²¹ A good solution to this drawback is to reduce the use of sonophotocatalysis to strictly produce more readily biodegradable intermediates that could be treated in a biological secondary step. In this way, complete mineralization of the organophosphate pesticide effluents may be achieved.

In this study, magnetic $\text{Fe}_3\text{O}_4@\text{SiO}_2@\text{TiO}_2$ nanocomposite was synthesized *via* a two-stage route. The catalytic activity of $\text{Fe}_3\text{O}_4@\text{SiO}_2@\text{TiO}_2$ NPs was evaluated by measuring COD_{Cr} removal efficiency of DDVP under UV light irradiation in self-made radial sonophotocatalytic reactor. Furthermore, the enhancement of biodegradability of DDVP by sonophotocatalysis was also studied.

Experimental

Materials and Reagents. All the reagents were of analytical grade and used without further purification. Iron(III) chloride hexahydrate (99%), tetraethyl orthosilicate (TEOS, 99%), tetrabutyl titanate (TBOT, 97%), anhydrous sodium acetate (NaAc), polyethylene glycol (PEG, $M_w = 4000$), *n*-hexane, ethylene glycol, ethanol, aqueous ammonia (25–28%), concentrated HCl, were purchased from Sinopharm Chemical Reagent Co., Ltd, China. Commercial DDVP were purchased from local market. Tap water was used in the radial sonophotocatalysis experiment and deionized water was used in the other experiment. The NdFeB magnet was purchased from Yingke (Beijing, China) with a cuboid shape of 50 mm × 50 mm × 5 mm and a surface magnetic field of 3000 G.

Preparation of Fe_3O_4 Nanoparticles. The Fe_3O_4 NPs were prepared according to the method previously reported by Zhao with tiny modification.^{13, 22} Briefly, $\text{FeCl}_3 \cdot 6\text{H}_2\text{O}$ (0.125 mol L^{-1}) were dissolved in ethylene glycol (80 mL), followed by the addition of NaAc (1.1 mol L^{-1}) and polyethylene glycol 4000 (25 mg mL^{-1}) into the system. The mixture was stirred vigorously for 60 min and then transferred into a Teflon-lined stainless-steel autoclave (100 mL). The autoclave was heated at 200 °C for 12 h and cooled at room temperature to form the black products. The products were washed several times with deionized water and ethanol

and then dried at 60 °C for 12 h in vacuum.

Preparation of $\text{Fe}_3\text{O}_4@\text{SiO}_2$ Nanoparticles. 0.2 g of as-prepared Fe_3O_4 was treated with 100 mL 0.1 M HCl solution followed by ultrasonication for 10 min. Subsequently, the treated Fe_3O_4 NPs were dispersed in the mixture solution of 160 mL of ethanol and 40 mL of H_2O . After adding 2.0 mL of aqueous ammonia (28%), the tetraethyl orthosilicate (TEOS, 120 μL) were added to the above mixture solution, respectively. The mixture solution were stirred at room temperature for 6 h to obtain the particles, and the particles were washed with deionized water and ethanol and then vacuum-dried the particles at 60 °C for 6 h.

Preparation of $\text{Fe}_3\text{O}_4@\text{SiO}_2@\text{TiO}_2$ Nanoparticles. The $\text{Fe}_3\text{O}_4@\text{SiO}_2$ NPs were coated in titanium dioxide *via* a solvothermal method. 0.2 g of $\text{Fe}_3\text{O}_4@\text{SiO}_2$ was re-dispersed in the mixture of 70 mL of hexane and 0.2 mL of deionized water, followed by the addition of tetrabutyl titanate (0.5 mL) under ultrasonication for 1 h. The mixture was transferred to Teflon-lined autoclave and keep at 100 °C for 3 h. The precipitates were collected and washed with hexane two or three times, then dried at room temperature. The powders were calcined at 500 °C for 3 h.

Characterization. X-ray diffraction (XRD) of the products were obtained on Shimadzu XRD-6000. The size and morphology of the core-shell NPs were observed in transmission electron microscope (TEM, JEM-2100 from JEOL Ltd) operating at an accelerating voltage of 200 kV. Sonophotocatalytic degradation experiments of commercial dichlorvos were carried out in a self-made radial sonophotocatalytic reactor.

Experimental Apparatus and Procedure. The radial sonophotocatalytic reactor had been reported in our previous study, which consists of radial-type ultrasound generator, a mechanical stirrer and a UV lamp placed perpendicular to the radial sonophotocatalytic reactor.²³ The ultrasound frequency was 20 kHz and the power output was 200 W. The power of the UV light was 500 W ($\lambda = 254 \text{ nm}$).

A desired concentration of DDVP was prepared by dissolving the 12 L of dechlorinated tap water aerated for 40 min at room temperature (19–25 °C). Then, the catalyst was added to the above DDVP solution. In order to reach the equilibrium adsorption of DDVP onto the catalyst surface, the suspension was stirred continuously in the dark for 30 min. Then, the solutions were irradiated under UV light and radial ultrasound in sonophotocatalytic reactor. Samples were taken at pre-selected time intervals using a pipette and the magnetic photocatalysts were removed immediately by a magnet. The supernatant solutions were obtained for analysis. The chemical oxygen demand (COD_{Cr}) was determined by the dichromate method (GB 11914-89). While 5-day biological oxygen demand (BOD_5) was determined by the dilution and seeding method (HJ 505-2009).

Results and Discussion

XRD Analysis. Figure 1 exhibits the XRD patterns of Fe_3O_4 , $\text{Fe}_3\text{O}_4@\text{SiO}_2$, and $\text{Fe}_3\text{O}_4@\text{SiO}_2@\text{TiO}_2$ (500 °C), respec-

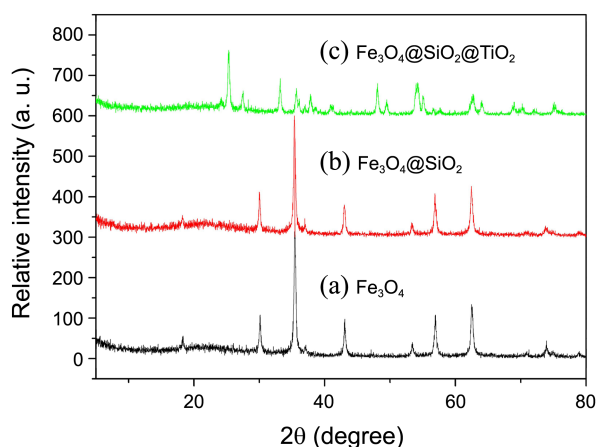


Figure 1. XRD pattern of (a) Fe_3O_4 ; (b) $\text{Fe}_3\text{O}_4@\text{SiO}_2$; (c) $\text{Fe}_3\text{O}_4@\text{SiO}_2@\text{TiO}_2$.

tively. As shown in Figure 1(a), the positions of all diffraction peaks match well with the standard JCPDS #841533 of Fe_3O_4 NPs, which indicate that the Fe_3O_4 NPs are single phase and belong to the cubic system. In Figure 1(b), it can be seen that the diffraction peaks of $\text{Fe}_3\text{O}_4@\text{SiO}_2$ are similar to those of the parent Fe_3O_4 , because of the amount of SiO_2 is small and they are mainly amorphous. Figure 1(c) exhibits the obvious XRD diffraction peaks at 25° , 38° , 48° , 54° , 55° , and 63° corresponding to (101), (004), (200), (105), (211), and (204), which are indexed to anatase TiO_2 (JCPDS #841285). The results supported that TiO_2 were successfully coated on the surface of $\text{Fe}_3\text{O}_4@\text{SiO}_2$. The presence of anatase phase is observed for $\text{Fe}_3\text{O}_4@\text{SiO}_2@\text{TiO}_2$ sample calcined at 500°C .

TEM Analysis. Figure 2 shows the TEM images of (a) Fe_3O_4 and (b) $\text{Fe}_3\text{O}_4@\text{SiO}_2$ as well as (c), (d) $\text{Fe}_3\text{O}_4@\text{SiO}_2@\text{TiO}_2$. Figure 2(a) shows the TEM image of Fe_3O_4 NPs. It can be seen that the shape of NPs is almost spherical with an average diameter of 190 nm. Figure 2(b) shows a TEM image of $\text{Fe}_3\text{O}_4@\text{SiO}_2$ NPs. The core-shell structure can be clearly distinguished because of the different colour contrast between the cores and shells. The $\text{Fe}_3\text{O}_4@\text{SiO}_2$ NPs are composed of magnetic cores with an average diameter of 190 nm and a silica shell with thickness of 10 nm on average. The thickness of the silica shell can be tuned by simply varying the amount of TEOS. Figure 2(c) shows that $\text{Fe}_3\text{O}_4@\text{SiO}_2@\text{TiO}_2$ NPs are monodisperse with a narrow size distribution of about 220 nm. Additionally, Figure 2(d) shows an HRTEM image of $\text{Fe}_3\text{O}_4@\text{SiO}_2@\text{TiO}_2$. It can be clearly found from Figure 2(d) that the lattice fringes of core are very different from the outer circles. The marked interplanar spacing of 0.351 nm corresponds well to that of the (101) lattice planes of anatase TiO_2 , while lattice fringe with interplanar spacing of 0.251 nm corresponds to the (311) planes of Fe_3O_4 core. The TiO_2 NPs with size of about 20 nm are observed. This implies that TiO_2 NPs are coated successfully on the surface of $\text{Fe}_3\text{O}_4@\text{SiO}_2$.

Effect of Added Amount of Catalyst on COD_{Cr} Removal Efficiency. To investigate the effect of the added amount of $\text{Fe}_3\text{O}_4@\text{SiO}_2@\text{TiO}_2$, initial catalyst concentration was varied

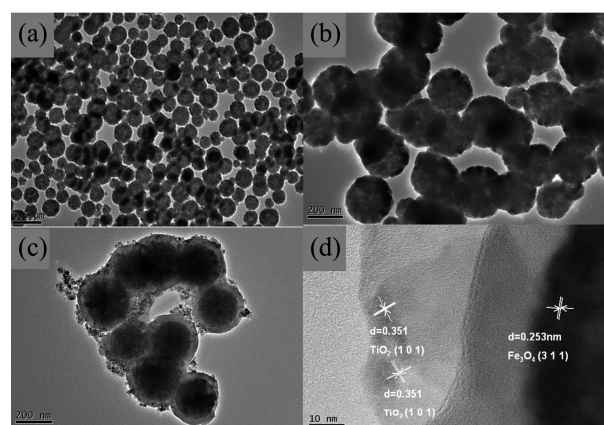


Figure 2. TEM images of (a) Fe_3O_4 , (b) $\text{Fe}_3\text{O}_4@\text{SiO}_2$, (c) $\text{Fe}_3\text{O}_4@\text{SiO}_2@\text{TiO}_2$ and (d) high-resolution TEM image of $\text{Fe}_3\text{O}_4@\text{SiO}_2@\text{TiO}_2$.

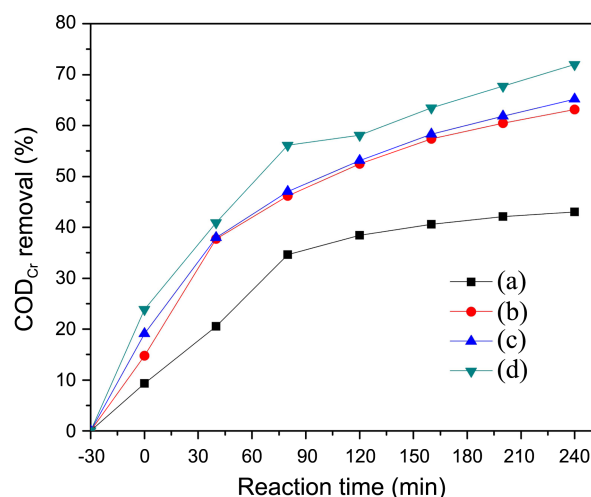


Figure 3. Effect of the amount of $\text{Fe}_3\text{O}_4@\text{SiO}_2@\text{TiO}_2$ on COD_{Cr} removal efficiency of DDVP by sonophotocatalysis. Initial $\text{COD}_{\text{Cr}} = 520 \text{ mg L}^{-1}$, 12 L, $\text{pH}=7.3$, ultrasound power 200 W, UV power 500 W, (a) 0.1 g L^{-1} , (b) 0.2 g L^{-1} , (c) 0.3 g L^{-1} , (d) 0.4 g L^{-1} .

in the range $0.1\text{--}0.4 \text{ g L}^{-1}$. Other experimental conditions were DDVP concentration 250 mg L^{-1} (initial $\text{COD}_{\text{Cr}} 520 \text{ mg L}^{-1}$) and $\text{pH} 7.3$. Figure 3 shows the degradation of in terms of COD_{Cr} removal. Before each experiment, the DDVP solutions and catalysts were first stirred for 30 min in the dark to reach an adsorption-desorption equilibrium. After 240 min reaction time, COD_{Cr} removal efficiency were 43%, 63.13%, 65.2% and 72% at the catalyst concentrations 0.1 g L^{-1} , 0.2 g L^{-1} , 0.3 g L^{-1} , and 0.4 g L^{-1} , respectively. It is seen that COD_{Cr} removal efficiency of DDVP increased with the increase catalyst concentration. The increase in COD_{Cr} removal efficiency of DDVP can be ascribed to an increase in the availability of the active sites with an increase in the catalyst concentration. However, increasing catalyst concentration above 0.2 g L^{-1} did not produce any significant improvement in COD_{Cr} removal efficiency of DDVP. This may be due to the aggregation of catalyst under high particle concentration, thus reducing light penetration.²⁴ Although the highest catalyst concentration (0.4 g L^{-1}) achieved the

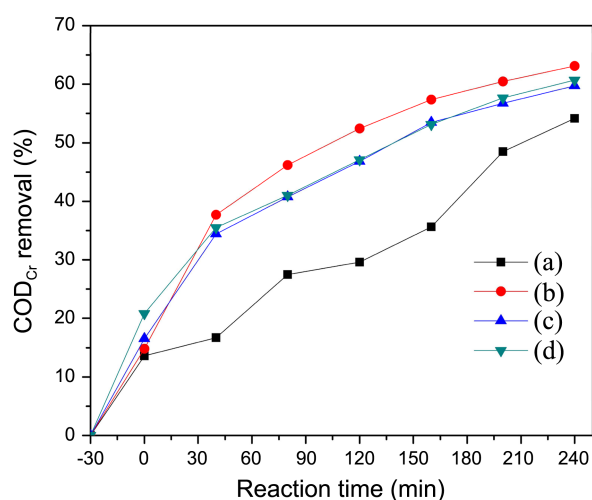


Figure 4. Effect of initial pH on COD_{Cr} removal efficiency of DDVP by sonophotocatalysis. Initial COD_{Cr} = 520 mg L⁻¹, 12 L, Fe₃O₄@SiO₂@TiO₂: 0.2 g L⁻¹, (a) pH=5.3, (b) pH=7.3, (c) pH=9.1, (d) pH=10.3.

best result, the concentration of 0.2 g L⁻¹ appeared to be the best condition investigated. Based on the results, the optimum catalyst concentration for degradation of DDVP pesticide is 0.2 g L⁻¹.

Effect of pH on COD_{Cr} Removal Efficiency. The solution pH is an important parameter because it determines the surface charge properties of the catalyst, the charge of the pollutant and the adsorption of the pollutant onto the catalyst surface.²⁵ The effect of pH on the sonophotocatalytic degradation of DDVP was investigated in the range of 5.3–10.3. In all the experiments the solution pH value was adjusted by the addition of H₂SO₄ or NaOH solutions of 0.1 M concentration. The experimental conditions were DDVP concentration 250 mg L⁻¹, the added amount of catalyst 0.2 g L⁻¹ and initial COD_{Cr} 520 mg L⁻¹. As shown in Figure 4, after 240 min of irradiation, the COD_{Cr} removal efficiency of DDVP were 54.19%, 63.13%, 59.74% and 60.70% at pH values of 5.3, 7.3, 9.1 and 10.3, respectively. Based on the results, it can be observed that the COD_{Cr} removal efficiency of DDVP is better at neutral pH than in acidic pH and alkaline pH. The effect of pH on the sonophotocatalytic reaction is generally attributed to the surface charge of TiO₂ and its relation with the ionic form of the organic compound (anionic or cationic).²⁶ Electrostatic attraction or repulsion between the catalyst's surface and the organic molecule is taking place and consequently enhances or inhibits, respectively, the sonophotocatalytic COD_{Cr} removal efficiency. The pollutant and thus the sonophotocatalytic degradation rates will be maximum near the point of zero charge of the catalyst as 6.8.^{27,28} This is in agreement with the higher COD_{Cr} removal efficiency observed for the DDVP under sonophotocatalysis at pH 7.3. Considering that dichlorvos is a unionizable compound, the increase of the reaction at alkaline pH can be ascribed to the high hydroxylation of the surface of the catalyst due to the presence of a large quantity of OH⁻ ions.²⁶ Consequently, higher concentrations of OH⁻

species are formed and the overall sonophotocatalytic degradation efficiency is enhanced. In Figure 4, it can be seen that for sonophotocatalysis at pH 10.3 and pH 7.3 present similar degradation extent. However, the pH of the solution was adjusted to 10.3 by the addition of NaOH. The consumption of chemical reagents is required, and making their extensive application difficult. Thus the pH 7.3 was selected as optimum pH. Moreover, the final pH after sonophotocatalytic treatment was 6.68 which is suitable for biological treatment.²⁹

Study on the Synergistic Effect. The degradation of commercial DDVP during sonocatalysis, photocatalysis and sonophotocatalysis was studied with an initial DDVP pesticide concentration of 250 mg L⁻¹ and a fixed of catalyst amount of 0.2 g L⁻¹. The COD_{Cr} removal efficiency obtained for the sonocatalytic, photocatalytic and sonophotocatalytic processes are presented in Figure 5. As shown in Figure 5, the COD_{Cr} removal efficiency of DDVP was equal to 63.13% with sonophotocatalysis in 240 min of reaction time. It was clear that the observed COD_{Cr} removal efficiency under sonophotocatalysis was much higher than that of photocatalysis or sonocatalysis. For photocatalysis and sonocatalysis, the COD_{Cr} removal efficiency of DDVP were equal to 59.47% and 45.9% after 240 min, respectively. These results indicated that radial ultrasound could enhance the photocatalytic efficiency of catalyst. This might be attributed to core-shell catalyst possessed a uniform size that could be dispersed in aqueous, which was useful for cleaning the surface of the catalyst by radial ultrasound. Meanwhile, the stability of the core-shell structural catalyst is very good in sonolysis. Moreover, radial ultrasound accelerated mass transfer of DDVP pesticide between the solution phase and the catalyst surface.³⁰

Sleiman *et al.* have reported the photocatalytic degradation of dichlorvos and showed that the degradation followed the general mechanism of photocatalytic degradation with the involvement of semiconductor electrons and holes.³¹

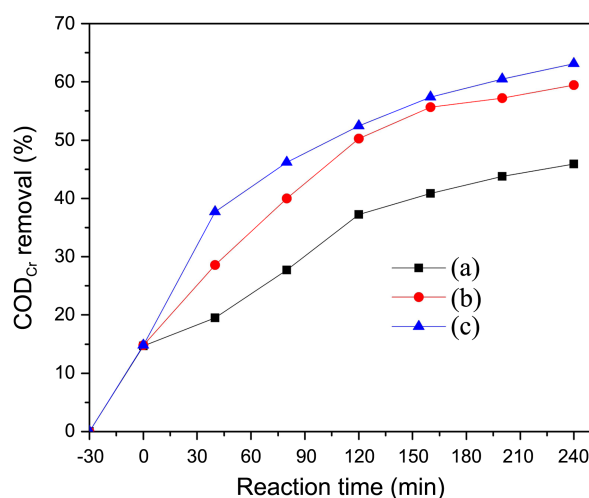


Figure 5. Effect of different processes on COD_{Cr} removal efficiency. (a) sonocatalysis, (b) photocatalysis, (c) sonophotocatalysis. Initial COD_{Cr} 520 mg L⁻¹, pH=7.3, Fe₃O₄@SiO₂@TiO₂: 0.2 g L⁻¹.

However, the simultaneous irradiation with both ultrasound and UV light in the presence of $\text{Fe}_3\text{O}_4@\text{SiO}_2@\text{TiO}_2$ showed an enhanced COD_{Cr} removal efficiency. The enhancement effect of ultrasound coupled to photocatalysis stems from the fact that ultrasound is deaggregating the magnetic catalyst, leading to an increase in its surface area and enhanced catalytic performance. Moreover, sonophotocatalysis increases the production of hydroxyl radicals in the reaction mixture arising from the sonolytic cleavage of water.

Study on the Biodegradability. The use of biological treatment is attractive due to its low operating cost, but the residence time is high. On the other hand, the degradation efficiency of advanced oxidation processes (AOP) is high, but the operation is relatively expensive due to the use of reagents and irradiation sources. Hence, the integration of sonophotocatalysis with existing biological processes would help in enhancing degradation rate, reducing residence time, and moderating operating costs. In order to evaluate the suitability of the photocatalytic and sonophotocatalytic treatment in commercial pesticide wastewater, the biodegradability tests were performed along the reaction time. When the ratio of $\text{BOD}_5/\text{COD}_{\text{Cr}}$ is more than 0.3, it was thought that the wastewater could be effectively degraded by biological treatment.^{32,33} For the untreated pesticide solution, the value of the $\text{BOD}_5/\text{COD}_{\text{Cr}}$ ratio was very low as 0.131, indicating that the sample was not biodegradable. In adsorption experiment the $\text{BOD}_5/\text{COD}_{\text{Cr}}$ ratio only increased from 0.131 to 0.138. No significant improvement of the biodegradability occurred. After 240 min reaction time, the values of $\text{BOD}_5/\text{COD}_{\text{Cr}}$ ratio were 0.411 for sonophotocatalytic and 0.37 for photocatalytic process, respectively. These results showed that the biodegradability of the treated wastewater was enhanced by using the sonophotocatalytic and photocatalytic process, converting the nonbiodegradable organic into more biodegradable compounds. Figure 6 shows that the biodegradability *via* sonophotocatalytic process is more enhanced than that of photocatalysis. In the case of sonophotocatalysis, the value of $\text{BOD}_5/\text{COD}_{\text{Cr}}$ ratio increased

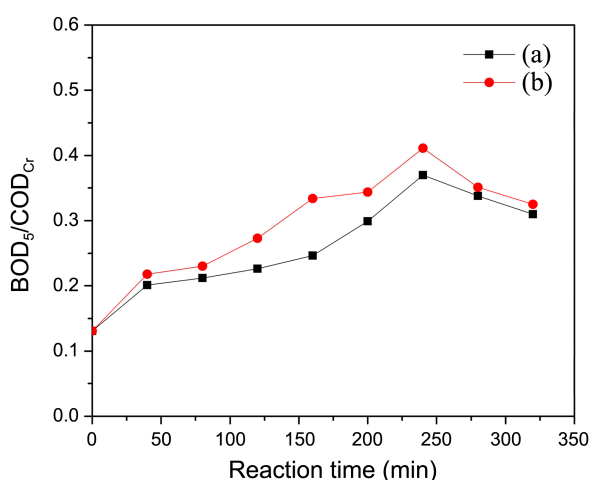


Figure 6. Biodegradability by different treatment processes, (a) photocatalysis, (b) sonophotocatalysis. Initial COD_{Cr} 520 mg L^{-1} , pH 7.3, $\text{Fe}_3\text{O}_4@\text{SiO}_2@\text{TiO}_2$: 0.2 g L^{-1} .

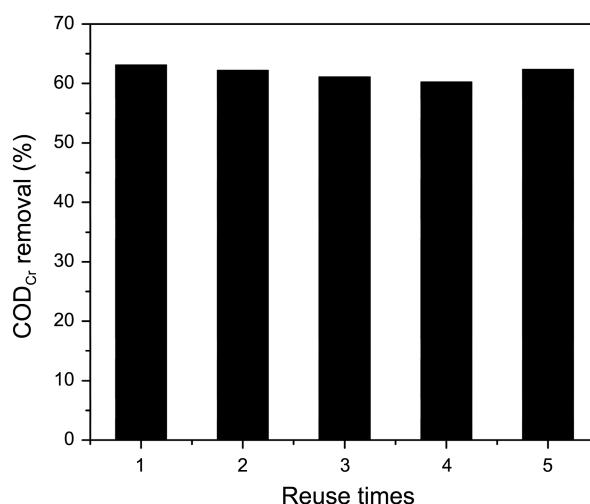


Figure 7. Effect of the reuse times of catalyst on COD_{Cr} removal efficiency of commercial DDVP. Experimental conditions: Initial $\text{COD}_{\text{Cr}} = 520 \text{ mg L}^{-1}$, $\text{Fe}_3\text{O}_4@\text{SiO}_2@\text{TiO}_2$: 0.2 g L^{-1} , 12 L, pH=7.3.

slowly, this might be attributed to the non-biodegradable pesticide molecule was not destroyed. However, it significantly improved after 160 min, this might be attributed to the part of pesticide molecule was destroyed, decomposed and even mineralized in the sonophotocatalytic process. When reaction at 240 min, the ratio of $\text{BOD}_5/\text{COD}_{\text{Cr}}$ increased to 0.411. Subsequently the ratio of $\text{BOD}_5/\text{COD}_{\text{Cr}}$ began to decrease, this might be due to there were some organic micro molecules which were difficult to biodegrade after the decomposition of DDVP pesticide. Therefore, pre-treatment time was an important factor to control the biodegradability of the commercial pesticide wastewater, and 240 min was appropriate for the sonophotocatalytic pre-treatment of practical wastewater.

Photocatalyst Stability and Reusability. The photocatalytic stability and reusability of the $\text{Fe}_3\text{O}_4@\text{SiO}_2@\text{TiO}_2$ photocatalyst were also studied with the commercial DDVP (250 mg L^{-1}) mixed with 0.2 g L^{-1} catalyst under sonophotocatalytic for 240 min. After the catalyst was used once, the catalyst was washed with deionized water and ethanol and then dried at $80 \text{ }^\circ\text{C}$ for 3 h and then reused in the next cycle without any calcinations treatment.

Figure 7 shows the COD_{Cr} removal efficiency of DDVP decreases from 63.13% on the first run to 60.74% on the 3rd cycle. It could be seen that the sonophotocatalytic activity of catalyst did not decrease conspicuously. This may be due to ultrasound continuously cleans the surface of the catalyst by acoustic cavitation, which is useful in maintaining its reactivity over longer irradiation times. After the 3rd cycle, the $\text{Fe}_3\text{O}_4@\text{SiO}_2@\text{TiO}_2$ catalyst was calcined at $500 \text{ }^\circ\text{C}$ for 3 h and reused. As shown in Figure 7, the original activity was recovered. Hence, calcination of the reused catalyst is necessary to regenerate the activity. After used for 5 times, the catalyst still maintain high photocatalytic activity, and the COD_{Cr} removal efficiency of DDVP decreases by 1.5% and the quantity loss of catalyst is less than 6%. It indicated that the $\text{Fe}_3\text{O}_4@\text{SiO}_2@\text{TiO}_2$ composite was highly stable

and reusable for continued use without losing its activity.

Conclusion

The Fe₃O₄@SiO₂@TiO₂ nanocomposite was prepared. The characterization results showed that the average diameter of Fe₃O₄ obtained was 190 nm, and the thickness of interlayer SiO₂ and outer layer TiO₂ were respectively 10 nm and 20 nm. The photocatalytic activity of Fe₃O₄@SiO₂@TiO₂ was examined by degrading DDVP under simulated radial ultrasound irradiation; the various operational factors (catalyst dosage, solution pH, and reaction time) were investigated. The optimal experimental conditions for the degradation of DDVP were a catalyst amount of 0.2 g L⁻¹ and a pH value of 7.3. Under optimal conditions, the COD_{Cr} removal efficiency in the sonophotocatalysis was much higher than photocatalysis or sonocatalysis. After used 5 times, the prepared catalysts also maintained high photocatalytic activity and catalyst recovery. Sonophotocatalysis could enhance the biodegradability of DDVP pesticide wastewater since the BOD₅/COD_{Cr} ratios increased from 0.131 to 0.411. The results indicate that the proposed sonophotocatalytic technology combining magnetic nanocomposite may be efficiently used in the pre-treatment of pesticide wastewater.

Acknowledgments. We greatly appreciate the Foundation of Provincial Natural Science Research Project of Anhui Colleges (KJ2014A059) and the Key Laboratory for Advanced Technology in Environmental Protection of Jiangsu Province (AE201107). J. He also thanks the support of the National Natural Science Foundation of China (21271008).

References

- Pirsaheb, M.; Fattahi, N.; Shamsipur, M. *Food Control* **2013**, *34*, 378.
- Naman, S. A.; Khammas, Z. A. A.; Hussein, F. M. *J. Photochem. Photobiol. A: Chem.* **2002**, *153*, 229.
- Senthilnathan, J.; Philip, L. *Chem. Eng. J.* **2011**, *172*, 678.
- Gomez, S.; Marchena, C. L.; Pizzio, L.; Pierella, L. *J. Hazard. Mater.* **2013**, *258*, 19.
- Cycoń, M.; Wójcik, M.; Piotrowska-Seget, Z. *Chemosphere* **2009**, *76*, 494.
- Schramm, J. D.; Hua, I. *Water Res.* **2001**, *35*, 665.
- Rotich, H. K.; Zhang, Z. Y.; Zhao, Y. S.; Li, J. C. *Intern. J. Environ. Anal. Chem.* **2004**, *84*, 289.
- Fujishima, A.; Honda, K. *Nature* **1972**, *238*, 37.
- Chen, X. B.; Mao, S. S. *Chem. Rev.* **2007**, *107*, 2891.
- Reyes-Gil, K. R.; Robinson, D. B. *ACS Appl. Mater. Interface* **2013**, *5*, 12400.
- Pozzo, R. L.; Baltanas, M. A.; Cassano, A. E. *Catal. Today* **1997**, *39*, 219.
- Polshettiwar, V.; Luque, R.; Fihri, A. Zhu, H.; Bouhrara, M., Basset, J. M. *Chem. Rev.* **2011**, *111*, 3036.
- Li, W.; Deng, Y. H.; Wu, Z. X.; Qian, X. F.; Yang, J. P.; Wang, Y.; Gu, D.; Zhang, F.; Tu, B.; Zhao, D. Y. *J. Am. Chem. Soc.* **2011**, *133*, 15830.
- Linley, S.; Leshuk, T.; Gu, F. X. *ACS Appl. Mater. Interfaces* **2013**, *5*, 2540.
- Yuan, Q.; Li, N.; Geng, W. C.; Chi, Y.; Li, X. T. *Mater. Res. Bull.* **2012**, *47*, 2396.
- Yang, J.; Cui, S. H.; Lian, H. Z. *Chinese J. Inorg. Chem.* **2013**, *29*, 2043.
- Fan, Y.; Ma, C.; Li, W.; Yin, Y. *Mat. Sci. Semicon. Proc.* **2012**, *15*, 582.
- Adeuyi, Y. G. *Environ. Sci. Technol.* **2005**, *39*, 8557.
- Taghizadeh, M. T.; Abdollahi, R. *Ultrason. Sonochem.* **2011**, *18*, 149.
- Ahmad, M.; Ahmed, E.; Hong, Z. L.; Ahmed, W.; Khalid, N. R. *Ultrason. Sonochem.* **2014**, *21*, 761.
- Liberatore, L.; Bressan, M.; Belli, C.; Lustrato, G.; Ranalli, G. *Water Air Soil Poll.* **2012**, *233*, 4751.
- Deng, Y. H.; Qi, D. W.; Deng, C. H.; Zhang, X. M.; Zhao, D. Y. *J. Am. Chem. Soc.* **2008**, *130*, 28.
- Shi, J. J.; Meng, L. R.; Hu, W.; He, J.; Hou, G. H. *Asian J. Chem.* **2014**, *26*, 1771.
- Prieto-Rodriguez, L.; Miralles-Cuevas, S.; Oller, I.; Agüera, A.; Puma, G. L.; Malato, S. *Appl. Catal. B: Environ.* **2012**, *128*, 119.
- Zhao, C.; Pelaez, M.; Duan, X.; Deng, H.; O'Shea, K.; Fatta-Kassinos, D. D. *Appl. Catal. B: Environ.* **2013**, *134-135*, 83.
- Evgenidou, E.; Fytianos, K.; Poullos, I. *Appl. Catal. B: Environ.* **2005**, *59*, 81.
- Gogate, P. R.; Pandit, A. B. *AIChE J.* **2004**, *50*, 1051.
- Kaur, S.; Singh, V. *Ultrason. Sonochem.* **2007**, *14*, 531.
- Singh, H. K.; Muneer, M.; Bahnmann, D. *Photochem. Photobiol. Sci.* **2003**, *2*, 151.
- Bokhale, N. B.; Bomble, S. D.; Dalbhanjan, R. R.; Mahale, D. D.; Hinge, S. P.; Banerjee, B. S.; Mohod, A. V.; Gogate, P. R. *Ultrason. Sonochem.* **2014**, *21*, 1797.
- Sleiman, M.; Ferronato, C.; Chovelon, J. M. *Environ. Sci. Technol.* **2008**, *42*, 3018.
- Badawy, M. I.; Gohary, F. E.; Ghaly, M. Y.; Ali, M. E. M. *J. Hazard. Mater.* **2009**, *169*, 673.
- Vera, I.; Sáez, K.; Vidal, G. *Environ. Technol.* **2013**, *34*, 2267.